

Article

Thermal Decomposition of Kraft Lignin under Gas Atmospheres of Argon, Hydrogen, and Carbon Dioxide

Qiangyu Yan ^{1,†}, Jinghao Li ^{2,†}, Jilei Zhang ^{1,*} and Zhiyong Cai ^{2,*}

¹ Department of Sustainable Bioproducts, Mississippi State University, Mississippi State, MS 39762, USA; yanqiangyu@gmail.com

² U.S. Department of Agriculture, Forest Service, Forest Products Laboratory, Madison, WI 53726, USA; jli@fs.fed.us

* Correspondence: jz27@msstate.edu (J.Z.); zcai@fs.fed.us (Z.C.); Tel.: +1-662-325-9413 (J.Z.); +1-608-231-9446 (Z.C.)

† These authors contributed equally to this work.

Received: 6 June 2018; Accepted: 28 June 2018; Published: 3 July 2018



Abstract: The behaviors of thermal decomposition of kraft lignin under three different gases (Ar, CO₂, or H₂) were analyzed and compared using a temperature-programmed decomposition-mass spectrometry (TPD-MS) system. Experimental results indicated that Ar atmosphere produced the highest yield of solid chars, while H₂ atmosphere generated the highest yield of liquids and CO₂ atmosphere had the highest yield of gases. TPD-MS results showed that H₂ atmosphere was consumed at the temperature range from 205 to 810 °C and CO₂ atmosphere was consumed at the temperature range from 185 to 1000 °C. The H₂ promoted the cleavage of lignin side chains and significantly enhanced the formation of CH₄, C₆H₆, HCHO, C₆H₅OH, CH₃OH, and tars. The percentages of water in produced liquids were 90.1%, 85.3%, and 95.5% for Ar, H₂, and CO₂ as atmosphere, respectively. The H₂ yielded more organic chemicals in produced liquids compared to the other two gases. The observed organic chemicals were mainly acetic acid, phenols, ketones, alcohols, aldehydes, and esters. BET surface areas of solid products were 11.3, 98.5, and 183.9 m²/g for Ar, H₂, and CO₂ as the atmosphere, respectively. C–H–O–N–S elemental and morphology analyses on solid products indicated that the lowest carbon content and the highest oxygen content were obtained if Ar atmosphere was used, while H₂ and CO₂ yielded more carbon in final solid products. Solid products obtained under CO₂ or H₂ atmosphere contained sphere-shaped nanoparticles.

Keywords: kraft lignin; thermal decomposition; H₂ atmosphere; CO₂ atmosphere

1. Introduction

Lignin is the second major component of lignocellulosic biomass and the most abundant aromatics biopolymer resource on earth [1,2]. Lignin is a byproduct produced from wood delignification and the pulping process; the global annual production of lignin is approximately more than 70 million metric tons [3,4]. The kraft process is the most widely used pulping process and kraft lignin accounts for more than 90% of the world's chemical pulp lignin production [5]. However, only 1–2% of lignin is isolated from wood pulping for commercial applications; the majority is burned onsite for heat and pulping chemical recovery [6]. With the increasing awareness of environmental issues and the depletion of fossil fuels, there is a tremendous research interest in utilizing biomass like lignin for the production of sustainable/renewable fuels and chemicals [7–12] and carbon-based nanomaterials like active carbons [13,14], carbon fibers [15], templated carbon [16], and graphene [17] through thermal conversion technologies.

The thermal decomposition of lignin has been extensively studied under an inert atmosphere using various techniques, such as thermogravimetric analysis (TGA) [18,19], Fourier-transform infrared spectroscopy (FTIR) [19,20], differential scanning calorimetry (DSC) [21], gas chromatography (GC)-mass spectrometer (MS) [22], and GC-nuclear magnetic resonance (NMR) [23], or the coupling of these characterization techniques [24,25]. The thermal decomposition process results in final products like volatiles, including low molecular gases (CO_2 , H_2O , CO , H_2) [18], light hydrocarbons (CH_4 , C_2H_6), aromatics, and oxygenates (CH_3OH , HCHO , and phenols), as well as liquids and solid char. The key factors affecting the property and distribution of the final products from thermal decomposition of lignin are heat treatment temperature, types of feedstock, feedstock particle size, and heating rate [26–28]. In addition, atmosphere used in the heating process affects the distribution of final products [29]. Up to date, most of literature reports the findings of thermal decomposition of lignin performed under inert atmospheres like He, Ar, or N_2 . Limited reports were found in relation to the thermal decomposition of lignin under reactive atmospheres such as CO_2 or H_2 [30].

Gasification of biomass under CO_2 atmosphere can convert solid carbon to CO -rich gas for the production of fuels [31]. In addition, hydrogasification of coal under H_2 atmosphere can significantly increase the yields of tar and liquid fuels [32]. Further studies on using different atmospheres such as CO_2 or H_2 for the decomposition of lignin can help provide better understanding of the mechanism involved in various thermal conversions of lignin. Therefore, the main purpose of this study was to investigate the effects of various gas atmospheres on the thermal decomposition process of kraft lignin. Specifically, the effect of three different gases (Ar, CO_2 , and H_2) on the yields of liquid, noncondensable gas, and solid carbon products, the formation of all volatiles and liquids, and the structures of solid carbon products of a thermal decomposition process of kraft lignin were investigated.

2. Materials and Methods

2.1. Materials

Kraft lignin (BioChoice, Plymouth, NC, USA) was supplied by Domtar Corp (Fort Mill, SC, USA). The proximate moisture analysis was carried out following ASTM D4442-07 standard [33]. According to the specification from Domtar, the BioChoice product contained 97.1 wt % of lignin. The ash content of lignin (1.65 wt %) was measured according to ASTM D1102 [34]. Lignin elemental analysis was carried out on a PE 2400 CHNS Elemental Analyzer (PerkinElmer, Waltham, MA, USA). The oxygen content was evaluated by the difference.

2.2. FTIR Spectroscopy

The FTIR spectrum of lignin was recorded with the PerkinElmer attenuated total reflection (ATR) spectrometer (PerkinElmer, Waltham, MA, USA) at a resolution of 2 cm^{-1} for 10 scans in 450 to 4000 cm^{-1} range to determine structural changes of kraft lignin during thermal decomposition.

2.3. Thermal Decomposition

The thermal decomposition of kraft lignin was performed in a fixed-bed reactor system composed of a stainless tubular reactor (1-inch O.D.) and condenser. For each experimental run, 5 grams of kraft lignin were loaded into the middle of the stainless tubular reactor. Each of three purging gases, Ar, H_2 , or CO_2 (purity $\geq 99.99\%$), was separately introduced into the system with a flow rate of 80 mL/min for 15 min, followed by raising the temperature to $1000\text{ }^\circ\text{C}$ at a ramping rate of $10\text{ }^\circ\text{C/min}$. After being held at $1000\text{ }^\circ\text{C}$ for 1 h, the furnace was turned off and allowed to cool to ambient temperature under the purging gas atmosphere. The solid and liquid products were collected from the system and weighed to calculate their mass distributions. The yield of gas products was calculated based on the differences among the three products yielded from the decomposing process.

The gaseous and volatile products released during the decomposition of kraft lignin under different atmosphere were continuously monitored and analyzed through an on-line residue gas

analyzer (RGA). The signals from the mass spectra of 2, 15, 28, 30, 31, 34, 44, 78, and 94 (m/z) were identified as the major contributors for specifically evolved gases and volatiles of H_2 , CH_4 , CO , $HCHO$, CH_3OH , H_2S , CO_2 , benzene, and phenol, respectively. Liquid products collected from the condenser were also analyzed and water content in the liquid products was measured using the Karl Fischer Titration. Water in liquid products was removed using isotropic distillation with toluene. The chemical composition of dewatered liquid products was performed using water-free basis using a gas chromatography/mass spectrometry analyzer (Agilent 6890, Agilent, Santa Clara, CA, USA). Elemental and surface area analyses were performed on solid products of kraft lignin thermally decomposed using a CHNS/O analyzer (Perkin Elmer PE2400 series II, PerkinElmer, Billerica, MA, USA) and an automatic adsorption unit (Autosorb-1, Quantachrome, Boynton Beach, FL, USA), respectively. The morphology of solid products was investigated using a scanning electron microscope (JEOL JSM-6500F Field Emission Scanning Electron Microscope, Peabody, St. Louis, MO, USA) operated with accelerating voltage of 5 kV. All SEM samples were precoated with 10 nm Pt before being introduced into the vacuum chamber.

3. Results and Discussion

3.1. FT-IR

Figure 1 shows the FT-IR spectrum of raw and thermally decomposed kraft lignin. There is a presence of a wide band at 3360 cm^{-1} observed in raw kraft lignin, indicating the presence of hydroxyl groups in phenolic and aliphatic structures (OH stretching vibration). There is also a range of signals around 2932 cm^{-1} (C–H stretchings in aromatic methoxyl groups as well as in methyl and methylene groups of side chains) and 2845 cm^{-1} (symmetric C–H stretching in $-CH_2-$ and tertiary C–H groups) typically found in lignin. The spectral region below 2000 cm^{-1} for raw kraft lignin is more difficult to analyze because most bands with contributions from various vibration modes are complex. In the carbonyl region, weak to medium bands are found at 1715 cm^{-1} that can be associated to unconjugated C=O, at 1638 cm^{-1} related to conjugated carbonyl/carboxyl spectra, and 1595 cm^{-1} corresponds to vibrations in the aromatic ring of lignin plus C=O stretching. A characteristic band at approximately 1510 cm^{-1} corresponds to benzene ring stretching vibrations for softwood lignin (Guaiacyl-G) [35]. The band at 1457 cm^{-1} is assigned to the asymmetric deformation of C–H bonds, while the band at 1420 cm^{-1} corresponds to the vibration of aromatic rings of lignin. The band at 1368 cm^{-1} represents the contribution of OH bendings of hydroxyl groups. A prominent band at 1264 cm^{-1} is assigned to C–O of guaiacyl rings, while the C–O stretching vibration in syringol rings is designated to the peak at 1217 cm^{-1} . A band at 1130 cm^{-1} is related to aromatic C–H in-plane deformation in guaiacyl rings, and a 1084 cm^{-1} band is assigned to C–O deformations of secondary alcohols and aliphatic ethers. The spectral region at 1033 cm^{-1} is because of aromatic C–H deformation and C–H out-of-plane vibrations. The FTIR spectra of thermally decomposed kraft lignin demonstrates that almost all the functional groups existing in raw kraft lignin have disappeared after going through the thermal decomposition at a high temperature.

3.2. Product Distribution

The summary of product yields (Figure 2) for the thermal decomposition process of kraft lignin indicates that argon atmosphere had the highest solid char yield of 36.5% among the three atmospheres evaluated, followed by H_2 with a yield of 23.0% and CO_2 with 15.1%. This can be explained by the fact that more components in kraft lignin were converted to liquid products or gases with reactive atmospheres like H_2 . Thermal decomposition of kraft lignin under H_2 atmosphere produced 28.4% liquid products, the highest yield among the three atmospheres, followed by 24.2% for Ar and 10.8% for CO_2 atmospheres. This is probably related to the conversion of oxygen in kraft lignin to water and organic compounds by hydrogen.

Figure 2 demonstrates that the thermal decomposition of kraft lignin under CO₂ atmosphere yielded the highest weight percentage value of 76.1% for gaseous phase, followed by 39.3% for Ar and 45.8% for H₂ atmospheres. The thermal decomposition of kraft lignin under CO₂ atmosphere produced less solid and liquid products and more gaseous products than under Ar and H₂ atmospheres because kraft lignin and its char are gasified by CO₂ at high temperature (>600 °C) [31].

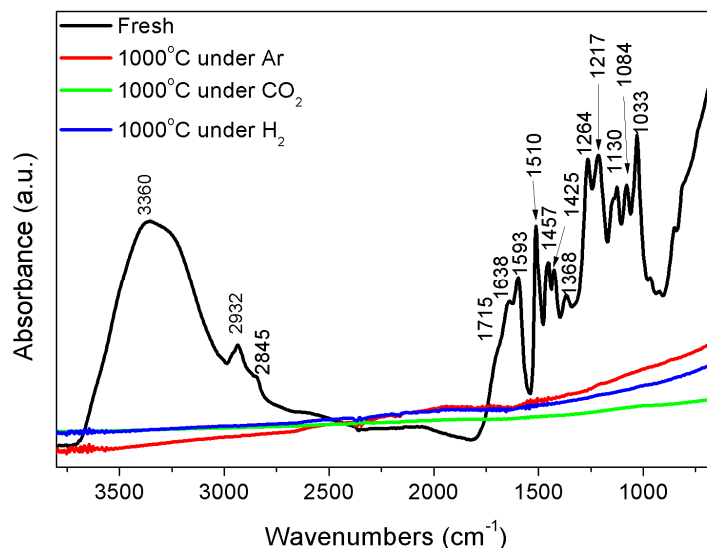


Figure 1. FTIR spectrum of raw and thermally decomposed kraft lignin.

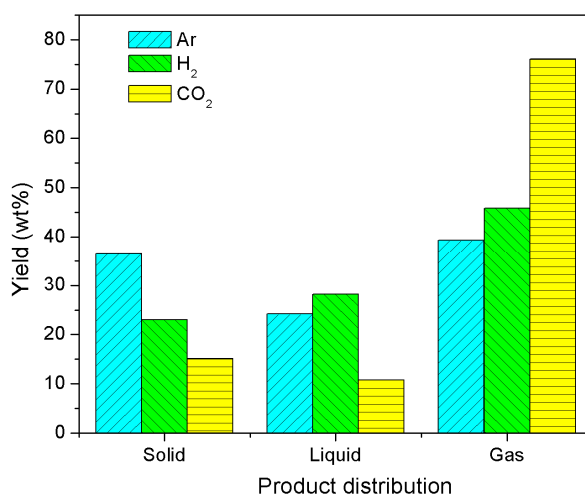


Figure 2. Products (solid carbon, liquid, and noncondensable gas) distribution of kraft lignin thermally decomposed using three different atmospheres at 1000 °C for 1 h.

3.3. Gas Evolution

Figure 3 summarizes typical gas profiles of H₂, CO₂, CH₄, and CO evolved from the thermal decomposition process of kraft lignin under three different atmospheres of Ar, H₂, and CO₂. Figure 4 is the summary of the evolution of major aromatic volatile compounds such as benzene (C₆H₆) and phenol (C₆H₅OH) from the decomposition of lignin oxygen-containing compounds, and methanol (CH₃OH) and formaldehyde (HCHO) from the cleavage of lignin side chains. Figure 5 shows the release of hydrogen sulfide (H₂S) from the thermal decomposition of kraft lignin. Table 1 summarizes the evolution temperature ranges and peak temperatures of all gas phases.

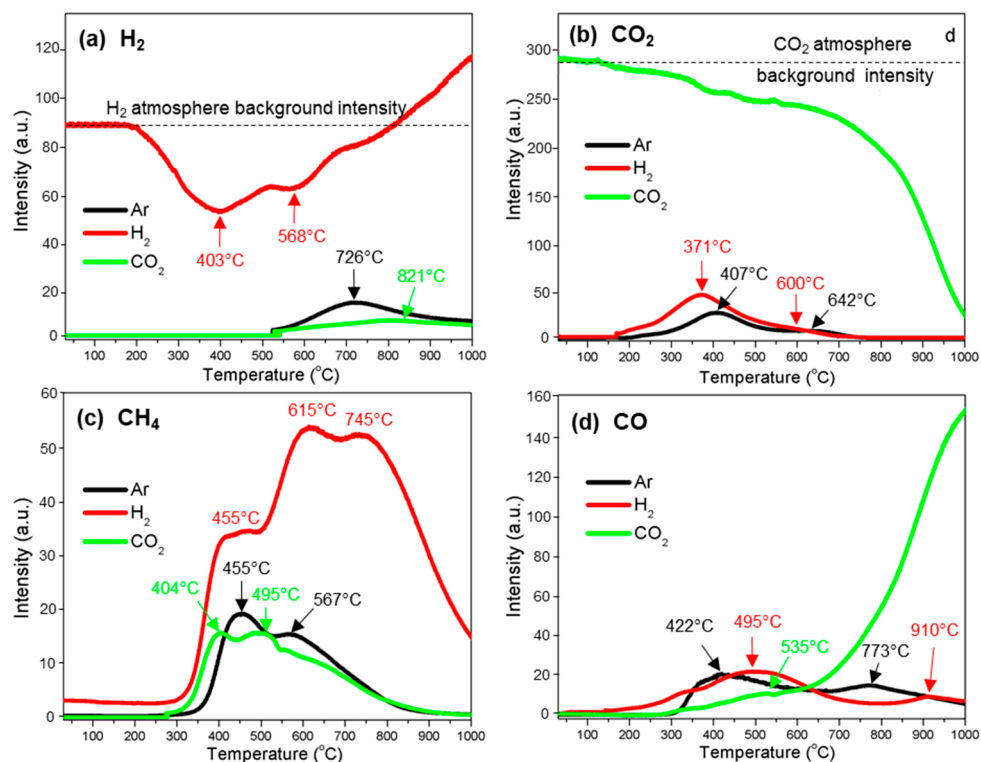


Figure 3. Gas evolution profiles of the thermal decomposition of kraft lignin under argon (Ar), hydrogen (H₂), and carbon dioxide (CO₂) atmospheres: (a) H₂; (b) CO₂; (c) CH₄; and (d) CO.

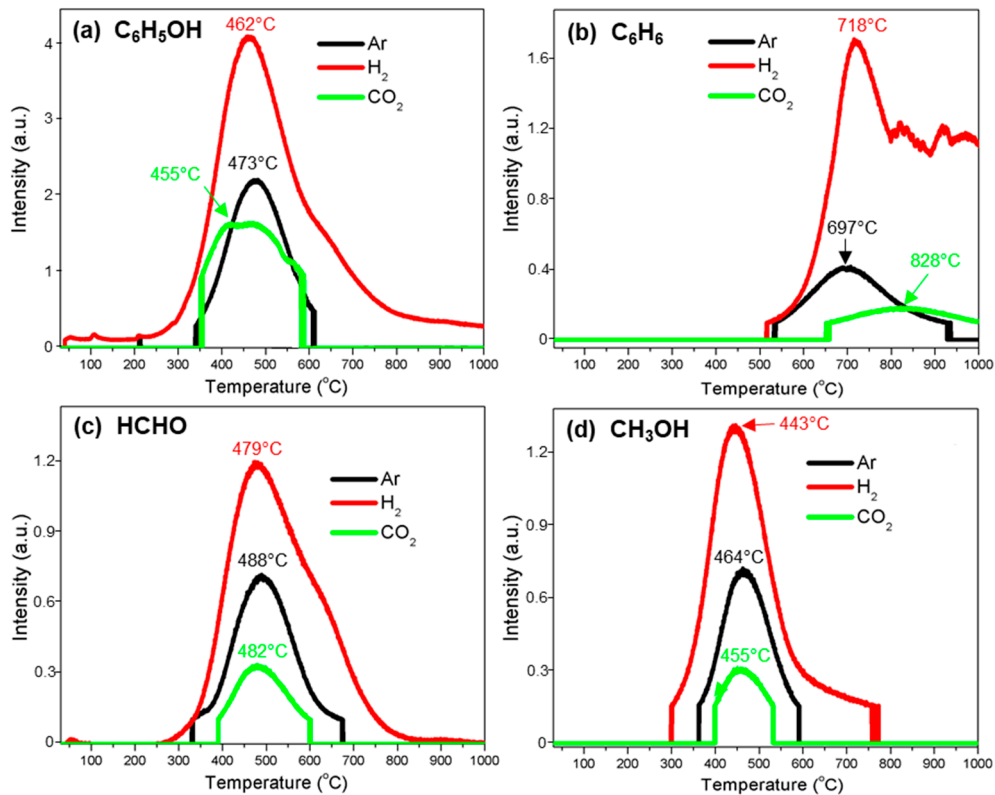


Figure 4. Gas evolution profiles of the thermal decomposition of kraft lignin under argon (Ar), hydrogen (H₂), and carbon dioxide (CO₂) atmospheres: (a) C₆H₅OH; (b) C₆H₆; (c) HCHO; and (d) CH₃OH.

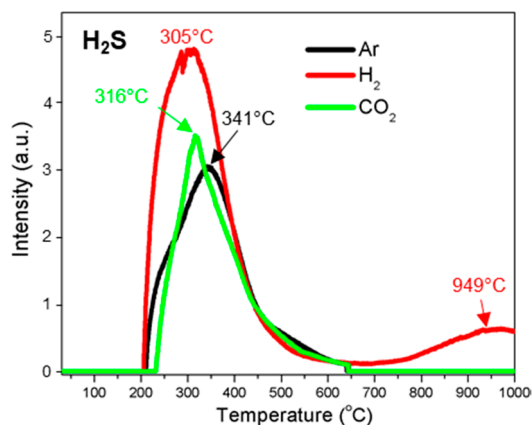


Figure 5. H₂S evolution profiles of the thermal decomposition of kraft lignin under argon (Ar), hydrogen (H₂), and carbon dioxide (CO₂) atmospheres.

Table 1. Summary of gas/volatile evolution temperature ranges and peak temperatures of thermal decomposition of kraft lignin under different atmospheres.

Gas/Volatile	Gas Atmosphere		
	Argon	Hydrogen °C	Carbon Dioxide
H ₂	522–1000 (722)	205–527 (403) * 527–800 (568) * 800–1000	821 (522–1000)
CO ₂	185–583 (407) 583–791 (642)	162–554 (371) 654–770 (600)	585–1000 *
CH ₄	236–532 (455) 532–915 (567)	268–495 (455) 495–688 (615) 688–1000 (745)	266–443 (404) 445–920 (495)
CO	246–679 (422) 679–1000 (773)	155–780 (495) 780–1000 (910)	279–547 (535) 547–1000 (1000)
C ₆ H ₅ OH	338–610 (473)	239–854 (462)	345–600 (445)
C ₆ H ₆	528–938 (697)	510–799 (718) 799–1000	656–1000 (828)
HCHO	329–678 (488)	249–850 (479)	390–601 (482)
CH ₃ OH	361–595 (464)	299–778 (443)	395–537 (455)
H ₂ S	210–646 (341)	199–656 (305) 704–1000 (949)	228–645 (316)

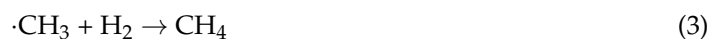
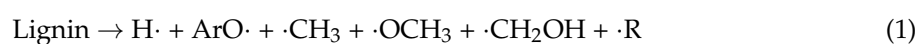
Note: “*” means values in parentheses are gas consumption.

3.3.1. H₂

Hydrogen presented in kraft lignin is in chemisorbed water as surface functionalities (e.g., carboxyl, phenolic groups) and bonds directly connected to carbon atoms as the part of aromatic or aliphatic structures. The carbon–hydrogen bond (C–H) is very stable but can be broken when heated at a high temperature. The thermal decomposition of kraft lignin in Ar atmosphere eliminates the part of hydrogen via thermal dissociation of C–H in aliphatic CH_x (x = 1–3) and aromatic rings [36]. The hydrogen formation temperature under Ar atmosphere (Figure 3a) started at 522 °C and reached its maximum at 726 °C. The H₂ evolution profile of thermal decomposition of kraft lignin under CO₂ atmosphere was similar to that of argon atmosphere. However, H₂ formation was suppressed in the

presence of CO₂ because of the reverse water-gas shift reaction (RWGSR) (CO₂ + H₂ = CO + H₂O [37]). In the reaction, the part of hydrogen from the thermal decomposition reaction of kraft lignin was consumed through RWGSR. The H₂ evolution curve under the H₂ atmosphere is dramatically different from these under Ar or CO₂. H₂ was firstly consumed by kraft lignin in the temperature ranges of 205–700 °C and then released from kraft lignin at the temperature range from 700 to 1000 °C.

Thermal decomposition of lignin generated various radicals such as phenoxy (ArO·), methyl (·CH₃), methoxy (·OCH₃), hydrogen atom (·H), and other fractional radicals (R) through reaction (1) [38]. Under H₂ atmosphere, these radicals can react with hydrogen molecules to form stable products like phenols (reaction (2)), methane (reaction (3)), methanol (reaction (4)), and other small compounds through radical processes. The hydrogen consumption was mainly ascribed to reactions (2) to (4) along with the formation of CH₄, CH₃OH, HCHO, and C₆H₅OH, etc. At temperatures above 700 °C, H₂ released from the decomposition process was because of the thermal cracking of the C–H bond in lignin chars and organic volatiles.



3.3.2. CO₂

The release of CO₂ exhibited two peaks (Figure 3b and Table 1). CO₂ mainly originated from the thermal decomposition of carboxyl (–COO[–]) and ester (–CO–O–R) groups [39]. The CO₂ release peak at lower temperatures (185–583 °C, centered at 407 °C) was because of decarboxylation reactions, while the cleavage of ether groups was predominantly responsible for the CO₂ evolution at higher temperatures (583–791 °C, centered at 642 °C). The evolution of CO₂ was significantly promoted under the hydrogen atmosphere compared to that under argon (i.e., two peaks shifted to lower temperatures, i.e., first peak to 371 °C and second peak to 600 °C). These phenomena were caused by the presence of hydrogen, which enhanced the cleavage of lignin side chains [19].

The purging gas CO₂ was consumed during the thermal decomposition under a carbon dioxide atmosphere (Figure 3b). At low temperatures, CO₂ might be consumed by active volatiles and solid residues to form various acids and ketones as previously reported [40], while the consumption of CO₂ at high temperatures (585 to 1000 °C) was because of the gasification reaction along with CO releasing (Figure 4d) as indicated by reaction (5):



3.3.3. CH₄

The evolution of CH₄ (Figure 3c) has two peaks as previously observed [41,42] (i.e., the first peak has a higher absorbance intensity at around 455 °C while the second peak has a relatively lower absorbance intensity at around 567 °C). The first CH₄ evolution peak was mainly caused by the cracking of weakly bonded methoxy groups (O–CH₃) [11,41,42] and the fragmentation of side aliphatic chains [41]. The evolution of CH₄ at high temperatures was because of the secondary pyrolysis of aromatic volatile intermediates [43,44] and the rearrangement of the lignin carbon skeleton along with CO release to remove the residual oxygen [41,42].

The CH₄ evolution profile under oxidizing CO₂ atmosphere was similar to that under argon atmosphere as previously observed [30], while the evolution peaks shifted to lower temperatures of 404 and 495 °C, respectively. This indicated that the presence of carbon dioxide accelerated the cracking of lignin methoxy and aliphatic groups. In addition, the CH₄ evolution at 800–1000 °C under

CO₂ atmosphere was higher than that under Ar atmosphere, suggesting that the reorganization of the lignin carbon skeleton was promoted by CO₂.

Three CH₄ evolution peaks at 455, 615, and 745 °C were observed during the thermal decomposition of kraft lignin under H₂ atmosphere (Figure 3c). The origin of the first two CH₄ evolution peaks was similar to those under Ar and CO₂ atmospheres. The third methane evolution peak occurred at higher temperatures between 680 and 1000 °C. Obviously, this new peak was related to the gasification of solid carbon by hydrogen. During this process, the residual carbon in lignin char reacted with hydrogen to produce methane as indicated by reaction (6):



3.3.4. CO

The evolution of CO occurred at a wide temperature range from 246 to 1000 °C (Figure 3d); this is because a number of functional groups could contribute to its formation. Two CO evolution peaks were observed under Ar atmosphere at 418 and 770 °C. The lower temperature CO evolution peak with a higher absorbance intensity was because of the rupture of weakly bonded ether (α -O-4 and β -O-4) bridges and the decarbonylation of the carbon on the C₃ side-chain [41,42,45], while the higher temperature CO evolution was mainly because of the cleavage of aromatic bonded oxygens (i.e., methoxy and phenolic groups) and the secondary cracking of oxygenate volatiles and tars [20,21,42].

Three CO evolution peaks (Figure 3d) were observed under hydrogen atmosphere, that is, the first was a shoulder peak from 155 to 362 °C, the second was stronger in intensity than the first, ranging from 362 to 780 °C with a maximum temperature at 495 °C, and the third, located at 910 °C, was because of the secondary reactions between volatiles and rearrangement of the char skeleton. Compared to CO formation peaks under argon, the first two peaks under hydrogen shifted to lower temperatures (i.e., the first peak to 362 °C and second peak to 495 °C). This indicated that the evolution of CO was significantly enhanced under a hydrogen flow.

Kraft lignin decomposition under CO₂ also offered three CO evolution peaks (Figure 3d). The first two peaks were similar to those of argon atmosphere. The third CO peak had a very strong evolution trend at about 1000 °C. This indicates that most of the lignin char residue was consumed by the gasification reactions ($\text{C}_s + \text{CO}_2 \rightleftharpoons 2\text{CO}$) to produce CO under CO₂ atmosphere.

3.3.5. Phenol (C₆H₅OH)

Under argon atmosphere, the phenol evolution from the thermal decomposition of kraft lignin was observed between the temperatures of 338 and 610 °C with a maximum temperature at 473 °C (Figure 4a). The formation of phenols is related to the dehydration of -OH groups in the alkyl side chain and the cleavage of ether bonds [41]. The C₆H₅OH evolution profile under oxidized CO₂ atmosphere was similar to that under Ar atmosphere, while the evolution peak shifted to a lower temperature at 455 °C because of the promoting effects of CO₂ on the lignin decomposition process. The C₆H₅OH evolution under hydrogen atmosphere occurred at a wide temperature range (239–854 °C) with a stronger intensity peak at 462 °C (Figure 4a). Under hydrogen atmosphere, phenoxy radicals ArO· can react with a hydrogen molecular to form a phenol molecular and a hydrogen atom, while generated hydrogen atoms can attack a phenoxy structure in a lignin molecule to form phenoxy radicals ArO·, therefore, more phenol products could be yielded under the hydrogen atmosphere.

3.3.6. Benzene (C₆H₆)

Under argon atmosphere, the evolution of benzene was detected in the temperature range from 528 to 938 °C with a maximum temperature at 697 °C (Figure 4b). The formation of benzene was because of the substantial cleavage of hydroxyl groups attached to aromatic rings. The formation of benzene under CO₂ atmosphere was suppressed at a lower temperature range from 528 to 840 °C, while promoted at a higher temperature range from 840 to 1000 °C. Lignin aromatic compounds

tended to be oxidized by CO₂ [11], and as a result, the formation of benzene was limited. On the other hand, the gasification of lignin char residues was responsible for the high evolution intensity of benzene in the temperature range from 840 to 1000 °C.

The evolution of benzene under a hydrogen flow was detected in the temperature range from 510 to 1000 °C with a maximum temperature at 718 °C. Moreover, the evolution of benzene reached a high and steady level when the temperature was above 799 °C because the formation of polycyclic aromatic hydrocarbons (PAHs) at high temperatures was promoted by hydrogen, while more C₆H₆ was generated simultaneously from the secondary cracking of PAHs.

3.3.7. Formaldehyde (HCHO)

The formation of HCHO under argon atmosphere mainly occurred between 329 and 678 °C with a maximum temperature at 488 °C (Figure 4c). The fragmentation of lignin side chains, for example, the cleavage of C_β–C_γ, is responsible for the HCHO evolution [39,40]. At carbon dioxide atmosphere, the HCHO evolution was suppressed because lignin side chains tended to be oxidized by CO₂ to form acids rather than HCHO.

The evolution of HCHO under hydrogen appeared at a very wide temperature range from 249 to 850 °C with a maximum temperature at 479 °C (Figure 4c), indicating that the formation of HCHO was significantly promoted under hydrogen. This was because hydrogen enhanced the cleavage of lignin side chains and promoted the reduction of acids (such as formic acid) to form more HCHO.

3.3.8. Methanol (CH₃OH)

The detected evolution temperature ranges of CH₃OH were 361–595, 395–537, and 299–778 °C (Figure 4d) for Ar, CO₂, and H₂ atmospheres, respectively. The cracking of aromatic methoxy (CH₃O–Ar) and aliphatic –CH₂OH groups were responsible for the formation of CH₃OH [39,40]. The formation of CH₃OH was suppressed under carbon oxidize but significantly promoted under hydrogen compared to argon atmosphere, which was the evolution behavior of HCHO. This phenomenon can be attributed to the oxidizing effects of carbon oxides and the reducing effects of hydrogen.

3.3.9. Hydrogen Sulfide (H₂S)

Sulfur is introduced to lignin through delignification reaction during a kraft pulping process, which results in sulfur presenting in lignin macromolecular structure as sulfate ions, elemental sulfur, adsorbed polysulfide, and/or organically bound sulfur. Lignin in general contains 2 to 3% sulfur after its kraft pulping process [46], but, kraft lignin used in this experiment contained less than 0.1% sulfur because the intensive acid purification step was applied in its production process. During a depolymerization process of lignin, sulfur is released in gas phases as dimethylsulfide (CH₃SCH₃), sulfur vapor, carbon disulfide (CS₂), carbonyl sulfide (COS), and/or hydrogen sulfide (H₂S) [47].

The trend of *m/z* 34 ion current was monitored as H₂S evolution during the decomposition of kraft lignin under three different atmospheres (Figure 5). Under argon atmosphere, H₂S evolution was observed in the temperature range from 210 to 646 °C with a maximum temperature of 341 °C. The evolution profile of H₂S under CO₂ atmosphere was similar to the one under Ar atmosphere, while the evolution peak shifted to a lower temperature of 316 °C. Two H₂S evolution peaks were observed during the thermal decomposition of kraft lignin under a hydrogen flow, that is, the first peak was at 305 °C, which was attributed by the depolymerization process, and the second one was at 949 °C; this peak was assigned to the reduction reaction of sulfur vapor (S + H₂ → H₂S) released from the depolymerization process. The presence of hydrogen significantly promoted the depolymerization of lignin and the reduction reaction of sulfur element in lignin.

3.4. Liquid Phase Analysis

The composition of liquid products collected from the thermal decomposition of kraft lignin under three different atmospheres are summarized in Table 2. The products were mainly aqueous phases, and the oil phase was negligible. Water was the major product in the final aqueous products, and its weight percentage in the final aqueous products was 90.1%, 85.3%, and 95.5% for Ar, H₂, and CO₂ atmospheres, respectively. The organic chemicals in the liquid samples are acetic acid, phenols, ketones alcohols, aldehydes, esters, and some nonidentified compounds.

Table 2. Summary of the composition of liquid products (wt %) collected from the thermal decomposition of kraft lignin under three different atmospheres.

Aqueous Phase Components	Ar	H ₂	CO ₂
Water content	90.1	85.3	95.5
Compounds in aqueous phase			
Acetic acid	27.8	25.5	29.1
Acetone	8.5	8.6	9.1
Hydroxyacetaldehyde	6.7	6.6	5.7
Methanol	2.5	4.5	2.1
Phenols	24.7	27.6	24.3
Other acids	8.5	6.1	10.7
Other alcohols	2.7	2.9	1.5
Other ketones	5.9	5.8	5
Other aldehydes	4.3	4.8	4
Esters	1.1	0.8	1.3
Nonidentified	7.3	6.8	7.2

3.5. Analysis and Characterization of Solid Products

Elemental analysis: Table 3 is the summary of the C–H–O–N–S elemental analysis performed on raw and thermally decomposed kraft lignin. The weight percentages of C, H, N, and S in unthermally treated kraft lignin are $65.2 \pm 0.2\%$, $6.1 \pm 0.2\%$, $0.1 \pm 0.05\%$, and $0.8 \pm 0.2\%$, respectively. The solid product of kraft lignin thermally treated under Ar has the lowest carbon content, while the one under CO₂ has the highest. Hydrogen weight percentages in solid products of kraft lignin thermally treated under Ar, H₂, and CO₂ are $0.9 \pm 0.1\%$, $1.0 \pm 0.2\%$, and $0.5 \pm 0.1\%$, respectively. No nitrogen was found in solid products of kraft lignin thermally treated. Sulfur was detected only from the solid product of kraft lignin thermally decomposed under argon flow. Oxygen contents are $1.8 \pm 0.5\%$ (under argon), $1.2 \pm 0.3\%$ (under hydrogen), and $1.5 \pm 0.3\%$ (under CO₂) for solid products of kraft lignin thermally treated under Ar, H₂, and CO₂, respectively.

Table 3. Summary of weight percentages (wt %) of C, H, O, N, and S in untreated kraft lignin and solid products of kraft lignin thermally decomposed under argon, hydrogen, and carbon dioxide at 1000 °C for 1 h.

Thermally Treated Condition	C	H	O	N	S
Untreated	65.2 ± 0.2	6.1 ± 0.2	27.4 ± 0.9	0.1 ± 0.05	0.8 ± 0.2
Under Ar	92.3 ± 0.7	0.9 ± 0.1	1.8 ± 0.5	-	0.1 ± 0.1
Under H ₂	96.3 ± 0.5	1.0 ± 0.2	1.2 ± 0.3	-	-
Under CO ₂	97.5 ± 0.5	0.5 ± 0.1	1.5 ± 0.3	-	-

BET surface area: Surface area analysis results indicate that the solid product of kraft lignin thermally treated under argon had the lowest surface area of $11.3 \text{ m}^2/\text{g}$, while the active atmosphere of CO₂ yielded the highest BET surface area of $183.9 \text{ m}^2/\text{g}$, followed by H₂, yielding the surface area of $98.5 \text{ m}^2/\text{g}$.

Morphology: Figure 6 shows SEM images of raw kraft lignin (Figure 6a) and solid products (Figure 6b–d) of kraft lignin thermally decomposed under three different atmospheres. The raw kraft lignin consisted of 1–2- μm particles. The surface of kraft lignin thermally decomposed under argon flow (Figure 6b) was smoother and cleaner. The solid product of kraft lignin thermally decomposed under CO_2 atmosphere (Figure 6c) was composed of sphere-shaped particles with their sizes ranging from 50 to 80 nm. Figure 6d shows the solid product of kraft lignin thermally decomposed under hydrogen atmosphere also had a large number of sphere-shaped nanoparticles with their sizes ranging from 50 to 100 nm.

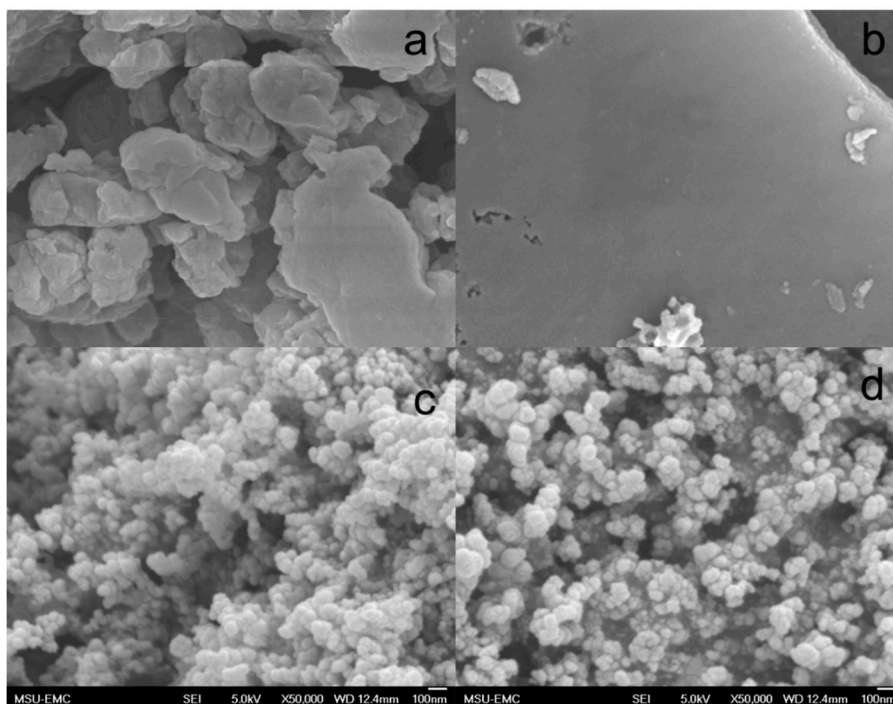


Figure 6. SEM images of raw kraft lignin (a) and solid products of kraft lignin thermally decomposed at 1000°C under three different atmospheres of Ar (b), CO_2 (c), and H_2 (d).

4. Conclusions

The effects of three different atmospheres of Ar, CO_2 , and H_2 on the products yielded from the process of the thermal decomposition of kraft lignin were examined by a temperature-programmed desorption-mass spectrometry (TPD-MS) system. Experimental results indicated that the thermal decomposition of kraft lignin under Ar atmosphere yielded the highest solid carbon products, while reactive CO_2 and H_2 atmospheres yielded the highest gas and liquid products, respectively. CO_2 mainly affected the thermal decomposition of kraft lignin at the high temperature range from 650 to 1000°C , where solid carbon was gasified to CO. Hydrogen was consumed at the temperature range from 205 to 810°C to form more CH_4 , C_6H_6 , HCHO, $\text{C}_6\text{H}_5\text{OH}$, H_2S , CH_3OH , and tars. Acetic acid, phenols, ketones, alcohols, aldehydes, and esters were detected in liquid products and more organic chemicals were produced under hydrogen atmosphere compared to the other two atmospheres. Solid carbon materials produced under reactive atmospheres (CO_2 or H_2) had higher surface areas. Solid products yielded under argon had the lowest carbon content and the highest oxygen content, while ones produced under hydrogen and carbon dioxide atmospheres contained more carbon. Solid products of kraft lignin thermally decomposed under CO_2 or H_2 atmosphere were composed of sphere-shaped nanoparticles.

Author Contributions: Conceptualization, Q.Y.; Methodology, Q.Y.; Formal Analysis, Q.Y. and J.L.; Investigation Q.Y. and J.L.; Data Curation, Q.Y. and J.L.; Writing-Original Draft Preparation, Q.Y.; Writing-Review & Editing, J.L., J.Z. and Z.C.; Supervision, J.Z. and Z.C.

Funding: This work was supported by the USDA Forest Service through Grant No.16-JV-1111124-075.

Acknowledgments: The authors would like to acknowledge Domtar Corp., North Carolina for providing kraft lignin for this study.

Conflicts of Interest: The authors declare no conflict of interest.

References

1. Isikgor, F.H.; Becer, C.R. Lignocellulosic biomass: A sustainable platform for the production of bio-based chemicals and polymers. *Polym. Chem.* **2015**, *6*, 4497–4559. [[CrossRef](#)]
2. Zhang, X.; Yan, Q.; Hassan, E.B.; Li, J.; Cai, Z.; Zhang, J. Temperature effects on formation of carbon-based nanomaterials from kraft lignin. *Mater. Lett.* **2017**, *203*, 42–45. [[CrossRef](#)]
3. Satheesh Kumar, M.N.; Mohanty, A.K.; Erickson, L.; Misra, M. Lignin and its applications with polymers. *J. Biobased Mater. Bioenergy* **2009**, *3*, 1–24. [[CrossRef](#)]
4. Zhang, X.; Yan, Q.; Li, J.; Zhang, J.; Cai, Z. Effects of physical and chemical states of iron-based catalysts on formation of carbon-encapsulated iron nanoparticles from kraft lignin. *Materials* **2018**, *11*, 139. [[CrossRef](#)] [[PubMed](#)]
5. Mahmood, N.; Yuan, Z.; Schmidt, J.; Xu, C. Production of polyols via direct hydrolysis of kraft lignin: Effect of process parameters. *Bioresour. Technol.* **2013**, *139*, 13–20. [[CrossRef](#)] [[PubMed](#)]
6. Zhang, X.; Yan, Q.; Leng, W.; Li, J.; Zhang, J.; Cai, Z.; Hassan, E.B. Carbon nanostructure of kraft lignin thermally treated at 500 to 1000 °C. *Materials* **2017**, *10*, 975. [[CrossRef](#)] [[PubMed](#)]
7. Lee, H.; Jae, J.; Ha, J.-M.; Suh, D.J. Hydro- and solvothermolysis of kraft lignin for maximizing production of monomeric aromatic chemicals. *Bioresour. Technol.* **2016**, *203*, 142–149. [[CrossRef](#)] [[PubMed](#)]
8. Li, C.; Zhao, X.; Wang, A.; Huber, G.W.; Zhang, T. Catalytic transformation of lignin for the production of chemicals and fuels. *Chem. Rev.* **2015**, *115*, 11559–11624. [[CrossRef](#)] [[PubMed](#)]
9. Li, Y.; Su, D.; Luo, S.; Jiang, H.; Qian, M.; Zhou, H.; Street, J.; Luo, Y.; Xu, Q. Pyrolysis gas as a carbon source for biogas production via anaerobic digestion. *RSC Adv.* **2017**, *7*, 41889–41895. [[CrossRef](#)]
10. Zakzeski, J.; Bruijninx, P.C.A.; Jongerius, A.L.; Weckhuysen, B.M. The Catalytic Valorization of Lignin for the Production of Renewable Chemicals. *Chem. Rev.* **2010**, *110*, 3552–3599. [[CrossRef](#)] [[PubMed](#)]
11. Yang, H.; Yan, R.; Chen, H.; Lee, D.H.; Zheng, C. Characteristics of hemicellulose, cellulose and lignin pyrolysis. *Fuel* **2007**, *86*, 1781–1788. [[CrossRef](#)]
12. Snell, G.J.; Huibers, D.T.A. Lignin Cracking Process Using Fast Fluidized Bed Reactions. U.S. Patent 4,409,416, 11 October 1982.
13. Rodríguez-Mirasol, J.; Bedia, J.; Cordero, T.; Rodríguez, J.J. Influence of Water Vapor on the Adsorption of VOCs on Lignin-Based Activated Carbons. *Sep. Sci. Technol.* **2005**, *40*, 3113–3135. [[CrossRef](#)]
14. Rodríguez-Mirasol, J.; Cordero, T.; Rodríguez, J.J. High-temperature carbons from kraft lignin. *Carbon* **1996**, *34*, 43–52. [[CrossRef](#)]
15. Hu, S.; Hsieh, Y.-L. Ultrafine microporous and mesoporous activated carbon fibers from alkali lignin. *J. Mater. Chem. A* **2013**, *1*, 11279. [[CrossRef](#)]
16. Ruiz-Rosas, R.; Valero-Romero, M.J.; Salinas-Torres, D.; Rodríguez-Mirasol, J.; Cordero, T.; Morallón, E.; Cazorla-Amorós, D. Electrochemical Performance of Hierarchical Porous Carbon Materials Obtained from the Infiltration of Lignin into Zeolite Templates. *ChemSusChem* **2014**, *7*, 1458–1467. [[CrossRef](#)] [[PubMed](#)]
17. Mun, S.P.; Cai, Z.; Zhang, J. Fe-catalyzed thermal conversion of sodium lignosulfonate to grapheme. *Mater. Lett.* **2013**, *100*, 180–183. [[CrossRef](#)]
18. Asadullah, M.; Rahman, M.A.; Ali, M.M.; Motin, M.A.; Sultan, M.B.; Alam, M.R.; Rahman, M.S. Jute stick pyrolysis for bio-oil production in fluidized bed reactor. *Bioresour. Technol.* **2008**, *99*, 44–50. [[CrossRef](#)] [[PubMed](#)]
19. Shen, D.K.; Gu, S.; Luo, K.H.; Wang, S.R.; Fang, M.X. The pyrolytic degradation of wood-derived lignin from pulping process. *Bioresour. Technol.* **2010**, *101*, 6136–6146. [[CrossRef](#)] [[PubMed](#)]
20. Cao, J.; Xiao, G.; Xu, X.; Shen, D.; Jin, B. Study on carbonization of lignin by TG-FTIR and high-temperature carbonization reactor. *Fuel Process. Technol.* **2013**, *106*, 41–47. [[CrossRef](#)]

21. Fox, S.C.; McDonald, A.G. Chemical and thermal characterization of three industrial lignins and their corresponding lignin esters. *BioResources* **2010**, *5*, 990–1009. [[CrossRef](#)]
22. Tsujiyama, S. Differential scanning calorimetric analysis of the lignin-carbohydrate complex degraded by wood-rotting fungi. *J. Wood Sci.* **2001**, *47*, 497–510. [[CrossRef](#)]
23. Chen, C.L. Characterization of lignin by oxidative degradation: Use of gas chromatography-mass spectrometry technique. *Meth. Enzymol.* **1988**, *161*, 110–136.
24. Kale, S.K.; Deshmukh, A.G.; Dudhare, M.S.; Patil, V.B. Microbial degradation of plastic: A review. *J. Biochem. Technol.* **2015**, *6*, 952–961.
25. Dobeles, G.; Rossinskaja, G.; Dizhbite, T.; Telysheva, G.; Meier, D.; Faix, O. Application of catalysts for obtaining 1,6-anhydrosaccharides from cellulose and wood by fast pyrolysis. *J. Anal. Appl. Pyrolysis* **2005**, *74*, 401–405. [[CrossRef](#)]
26. Predel, M.; Kaminsky, W. Pyrolysis of rape-seed in a fluidised-bed reactor. *Bioresour. Technol.* **1998**, *66*, 113–117. [[CrossRef](#)]
27. Heo, H.S.; Park, H.J.; Yim, J.-H.; Sohn, J.M.; Park, J.; Kim, S.-S.; Ryu, C.; Jeon, J.-K.; Park, Y.-K. Influence of operation variables on fast pyrolysis of *Miscanthus sinensis* var. purpurascens. *Bioresour. Technol.* **2010**, *101*, 3672–3677. [[CrossRef](#)] [[PubMed](#)]
28. He, R.; Ye, X.P.; English, B.C.; Satrio, J.A. Influence of pyrolysis condition on switchgrass bio-oil yield and physicochemical properties. *Bioresour. Technol.* **2009**, *100*, 5305–5311. [[CrossRef](#)] [[PubMed](#)]
29. Brebu, M.; Tamminen, T.; Spiridon, I. Thermal degradation of various lignins by TG-MS/FTIR and Py-GC-MS. *J. Anal. Appl. Pyrolysis* **2013**, *104*, 531–539. [[CrossRef](#)]
30. Shen, D.; Hu, J.; Xiao, R.; Zhang, H.; Li, S.; Gu, S. Online evolved gas analysis by Thermogravimetric-Mass Spectroscopy for thermal decomposition of biomass and its components under different atmospheres: Part I. Lignin. *Bioresour. Technol.* **2013**, *130*, 449–456. [[CrossRef](#)] [[PubMed](#)]
31. Yan, Q.; Toghiani, H.; Yu, F.; Cai, Z.; Zhang, J.; Yan, Q. Effects of pyrolysis conditions on yield of bio-chars from pine chips. *For. Prod. J.* **2011**, *61*, 367–371. [[CrossRef](#)]
32. Mamoru Kaiho, Y.T. Change in thermoplastic properties of coal under pressure of various gases. *Fuel* **1979**, *58*, 397–398. [[CrossRef](#)]
33. ASTM D4442-07(2007). *Standard Test Methods for Direct Moisture Content Measurement of Wood and Wood-Based Materials*; ASTM Int.: West Conshohocken, PA, USA, 2007.
34. ASTM D1102-84(2007). *Standard Test Method for Ash in Wood*; ASTM Int.: West Conshohocken, PA, USA, 2007.
35. Faix, O. Classification of lignins from different botanical origins by FT-IR spectroscopy. *Holzforschung* **1991**, *45*, 21–27. [[CrossRef](#)]
36. Brebu, M.; Vasile, C. Thermal degradation of lignin—A review. *Cellul. Chem. Technol.* **2010**, *44*, 353–363.
37. Yamaguchi, A.; Mimura, N.; Shirai, M.; Sato, O. Bond cleavage of lignin model compounds into aromatic monomers using supported metal catalysts in supercritical water. *Sci. Rep.* **2017**, *7*, 46172. [[CrossRef](#)] [[PubMed](#)]
38. Tsuchiya, K.; Huang, J.D.; Tominaga, K.I. Reverse Water-Gas Shift Reaction Catalyzed by Mononuclear Ru Complexes. *ACS Catal.* **2013**, *3*, 2865–2868. [[CrossRef](#)]
39. Wang, S.; Lin, H.; Ru, B.; Sun, W.; Wang, Y.; Luo, Z. Comparison of the pyrolysis behavior of pyrolytic lignin and milled wood lignin by using TG-FTIR analysis. *J. Anal. Appl. Pyrolysis* **2014**, *108*, 78–85. [[CrossRef](#)]
40. Zhang, H.; Xiao, R.; Wang, D.; He, G.; Shao, S.; Zhang, J.; Zhong, Z. Biomass fast pyrolysis in a fluidized bed reactor under N₂, CO₂, CO, CH₄ and H₂ atmospheres. *Bioresour. Technol.* **2011**, *102*, 4258–4264. [[CrossRef](#)] [[PubMed](#)]
41. Wang, S.; Wang, K.; Liu, Q.; Gu, Y.; Luo, Z.; Cen, K.; Fransson, T. Comparison of the pyrolysis behavior of lignins from different tree species. *Biotechnol. Adv.* **2009**, *27*, 562–567. [[CrossRef](#)] [[PubMed](#)]
42. Liu, Q.; Wang, S.; Zheng, Y.; Luo, Z.; Cen, K. Mechanism study of wood lignin pyrolysis by using TG-FTIR analysis. *J. Anal. Appl. Pyrolysis* **2008**, *82*, 170–177. [[CrossRef](#)]
43. Kishimoto, T.; Uraki, Y.; Ubukata, M. Chemical synthesis of β-O-4 type artificial lignin. *Org. Biomol. Chem.* **2006**, *4*, 1343–1347. [[CrossRef](#)] [[PubMed](#)]
44. Babij, N.R.; McCusker, E.O.; Whiteker, G.T.; Canturk, B.; Choy, N.; Creemer, L.C.; Amicis, C.V.D.; Hewlett, N.M.; Johnson, P.L.; Knobelsdorf, J.A.; et al. NMR chemical shifts of trace impurities: Industrially preferred solvents used in process and green chemistry. *Org. Process Res. Dev.* **2016**, *20*, 661–667. [[CrossRef](#)]

45. Zhao, J.; Xiuwen, W.; Hu, J.; Liu, Q.; Shen, D.; Xiao, R. Thermal degradation of softwood lignin and hardwood lignin by TG-FTIR and Py-GC/MS. *Polym. Degrad. Stab.* **2014**, *108*, 133–138. [[CrossRef](#)]
46. Sjostrom, E. *Wood Chemistry: Fundamentals and Applications*; Elsevier: Amsterdam, The Netherlands, 2013; ISBN 978-0-08-092589-9.
47. Dondi, D.; Zeffiro, A.; Speltini, A.; Tomasi, C.; Vadivel, D.; Buttafava, A. The role of inorganic sulfur compounds in the pyrolysis of Kraft lignin. *J. Anal. Appl. Pyrolysis* **2014**, *107*, 53–58. [[CrossRef](#)]



© 2018 by the authors. Licensee MDPI, Basel, Switzerland. This article is an open access article distributed under the terms and conditions of the Creative Commons Attribution (CC BY) license (<http://creativecommons.org/licenses/by/4.0/>).